Quasi-two-dimensional NaCl crystals encapsulated between graphene sheets and their decomposition under an electron beam

Lehnert, T.; Kretschmer, S.; Bräuer, F.; Krasheninnikov, A.; Kaiser, U.;

Originally published:

November 2021

Nanoscale 13(2021), 19626-19633

DOI: https://doi.org/10.1039/D1NR04792B

Nanoscale

Accepted Manuscript

This article can be cited before page numbers have been issued, to do this please use: T. Lehnert, S. Kretschmer, F. Bräuer, A. V. Krasheninnikov and U. Kaiser, *Nanoscale*, 2021, DOI: 10.1039/D1NR04792B.

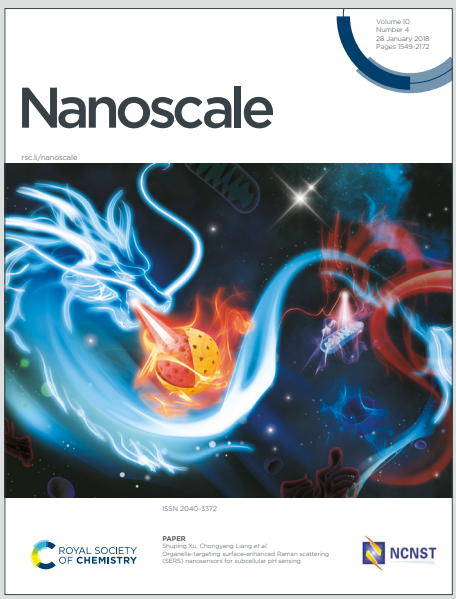

ROYAL SOCIETY OF CHEMISTRY

rsc.li/nanoscale

View Article Online
DOI: 10.1039/D1NR04792B

ARTICLE

Quasi-Two-Dimensional NaCl Crystals Encapsulated Between Graphene Sheets and their Decomposition under the Electron Beam

Received 00th January 20xx,
Accepted 00th January 20xx

DOI: 10.1039/x0xx00000x

Tibor Lehnert, †*[a,b] Silvan Kretschmer, [c] Fredrik Bräuer,[a] Arkady V. Krasheninnikov[c,d] and Ute Kaiser*[a]

Quasi-two-dimensional (2D) sodium chloride (NaCl) crystals of various lateral sizes between graphene sheets were manufactured via supersaturation from a saline solution. Aberration-corrected transmission electron microscopy was used for systematic in-situ investigations of the crystals and their decomposition under an 80 kV electron beam. Counterintuitively, bigger clusters were found to disintegrate faster under electron irradiation, but in general no correlation between crystal sizes and electron doses at which the crystals decompose was found. As for the destruction process, an abrupt decomposition of the crystals was observed, which can be described by a logistic decay function. Density-functional theory molecular dynamics simulations provide insights into the destruction mechanism, and indicate that even without account for ionization and electron excitations, free-standing NaCl crystals must quickly disintegrate due to ballistic displacement of atoms from their surface and edges during imaging. However, graphene sheets mitigate damage development by stopping the displaced atoms and enable the immediate recombination of defects at the surface of the crystal. At the same time, once a hole in graphene appears, the displaced atoms escape, giving rise to the quick destruction of the crystal. Our results provide quantitative data on the stability of encapsulated quasi 2D NaCl crystals under electron irradiation and allow to conclude that only high-quality graphene is suitable for protecting ionic crystals from beam damage in electron microscopy studies.

A Introduction

Graphene is frequently used as a support material in high-resolution transmission electron microscopy (TEM) due to its mechanical strength,[1] high electrical and thermal conductivity,[2–4] thinness, chemical inertness[5,6] and the high electron radiation resistance at electron energies up to 80 keV.[7,8] Moreover, encapsulation of materials inside graphene sheets allow in-situ studies of radiation- and environment-sensitive systems with TEM.[8–13] Remarkably, not only solid materials, e.g., two-dimensional (2D) transition metal dichalcogenides[14–17], but also liquids can be encapsulated between graphene sheets and investigated in TEM. The former systems with a 'sandwich' geometry are normally referred to as vertical heterostructures,[17] while the term graphene liquid cells (GLCs)[18] is normally used for the latter.

The behaviour of the encapsulated materials is frequently governed by the electron beam.[19,20] Interactions between the electron beam and a specimen can be split into two main categories.[21] First, the electron-nucleus interaction in which the atom is displaced by momentum transfer of the energetic electron, the so-called knock-on damage mechanism, and second, the electron-electron interaction described by inelastic scattering processes in which the valence electrons of the atom are excited (radiolysis) or even removed (ionization).[21–23]

Defects can also appear through chemical etching. This can be caused by reactive species left at the sample surface after its preparation or present in the TEM column.[24] The process can be facilitated by the electron beam. The residues such as oxygen molecules can undergo bond scission by ionization resulting in formation of radicals, which in turn attack the sample surface.[25,26] Chemical etching is very likely to be the main mechanism to damage in graphene at beam energies below 80 keV.[27,28] It was shown that metal and vapor-mediated etching primarily takes place at defect sites or starts at contaminated areas and not on the pristine graphene lattice.[29,30]

At the same time, the stability and mechanisms of radiation damage in the materials encapsulated between graphene sheets are not fully understood yet. In particular, ionic crystals (such as NaCl) are sensitive to radiation damage,[31,32] which should lead to the formation of chlorine radicals and promote chemical etching of graphene. It is therefore astonishing that graphene enclosures are

[a] Electron Microscopy Group of Materials Science, Ulm University, 89081 Ulm, Germany.
[b] Institute for Quantum Optics, Ulm University, 89081 Ulm, Germany.
[c] Institute of Ion Beam Physics and Materials Research, Helmholtz-Zentrum Dresden-Rossendorf, 01328 Dresden, Germany.
[d] Department of Applied Physics, Aalto University, P.O. Box 11100, 00076 Aalto, Finland.
*corresponding authors: tibor.lehnert@gmail.com, ute.kaiser@uni-ulm.de
†Now at: Laboratory for Electron Microscopy, Karlsruhe Institute of Technology (KIT), 76131 Karlsruhe, Germany
‡ Electronic Supplementary Information (ESI) available: See DOI: 10.1039/x0xx00000x; Experimental TEM data can be accessed at DOI: http://dx.doi.org/10.18725/OPARU-39292

stable and the encapsulated ionic crystals can be imaged in a TEM,[8,33–35] although they eventually get destroyed. Thus, it is highly desirable to understand at the microscopic level what governs the stability of the system under electron beam.

Here, we apply spherical aberration (Cs)-corrected high-resolution (HR)TEM imaging at 80 kV to analyse the degradation process of very thin, quasi 2D NaCl crystals encapsulated between graphene sheets and rationalize the results through first-principles simulations.

B Results and Discussions

As seen in Fig. 1, cubic quasi 2-dimensional NaCl crystals have been formed within the GLC, which is attributed to supersaturation of sodium cations and chlorine anions in the liquid, identical to the previously observed NaCl crystals between graphene layers[36]. We observed NaCl crystals with thicknesses in the range of 4-8 layers (see Supporting Information for thickness estimation). In all our TEM experiments, the projected size of the crystals did not change at all initially, i.e., the encapsulated NaCl crystals did not disintegrate immediately under the electron beam. The typical NaCl crystal shown in Fig. 1 has a projected size of ~220 nm^2 and the images were taken with a dose rate of ~$6.1 \cdot 10^5$ e^-/nm^2s. Fig. 1 (a) shows the raw HRTEM images illustrating the degradation process and in Fig. 1 (b) the images are colour coded for better visualization of different layers. The two encapsulating graphene layers are marked red and blue, respectively, and the NaCl crystal is coloured green. The same colours are used in the FFT in Fig. 1(a). When the sample is exposed to the electron beam, the crystal was stable for 533 s, then it started to decompose. We observed that the decomposition was accompanied by the formation of a hole in one of the protecting graphene layers (encircled white). We note that the visualization of defects in graphene facing the encapsulated system is difficult with optical filtering methods because of the low contrast of graphene as compared to that of NaCl crystals, but they can clearly be identified by naked eye inspection of the images.

In our experiments the NaCl crystals started to decompose around a hole in graphene, which allowed to assume that the encapsulated NaCl crystals are only stable as long as the graphene sheet is undamaged. It is likely that creation of even a single point defect in graphene is sufficient to induce the decomposition of the NaCl crystal as the damaged graphene is more susceptible for further degradation[37] and the hole will grow up due to chemical etching induced by the chlorine radicals formed by the interaction of NaCl with the electron beam and/or a reduced knock-on damage threshold in graphene at the defect position[38]. Impurities, e.g., the three dark particles seen next to the NaCl crystal, were found to have no influence on NaCl degradation.

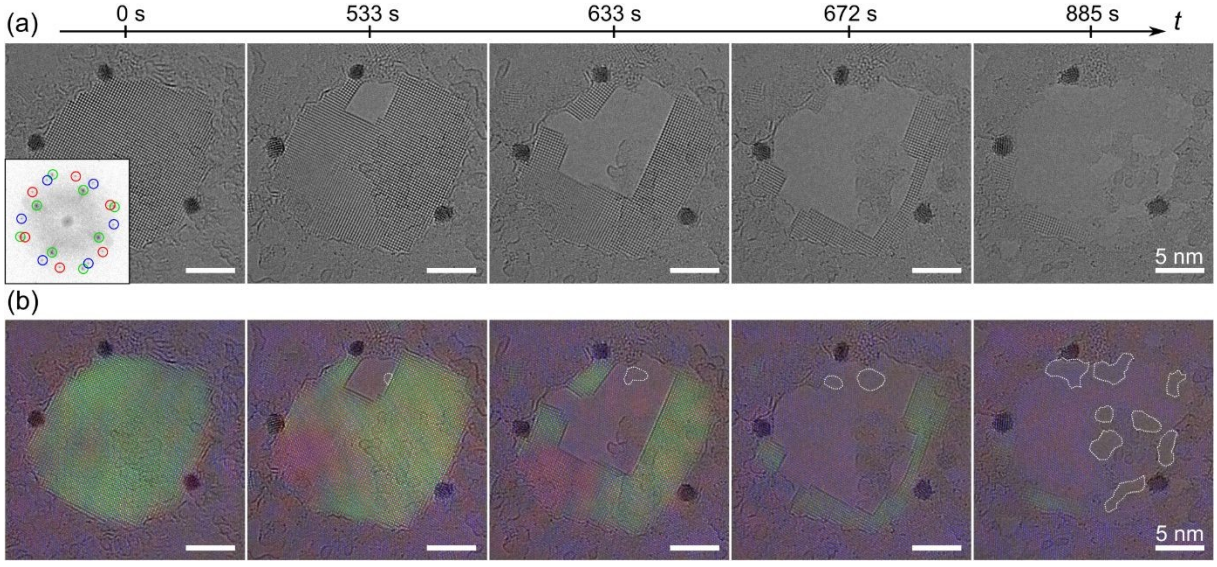

View Article Online
DOI: 10.1039/D1NR04792B

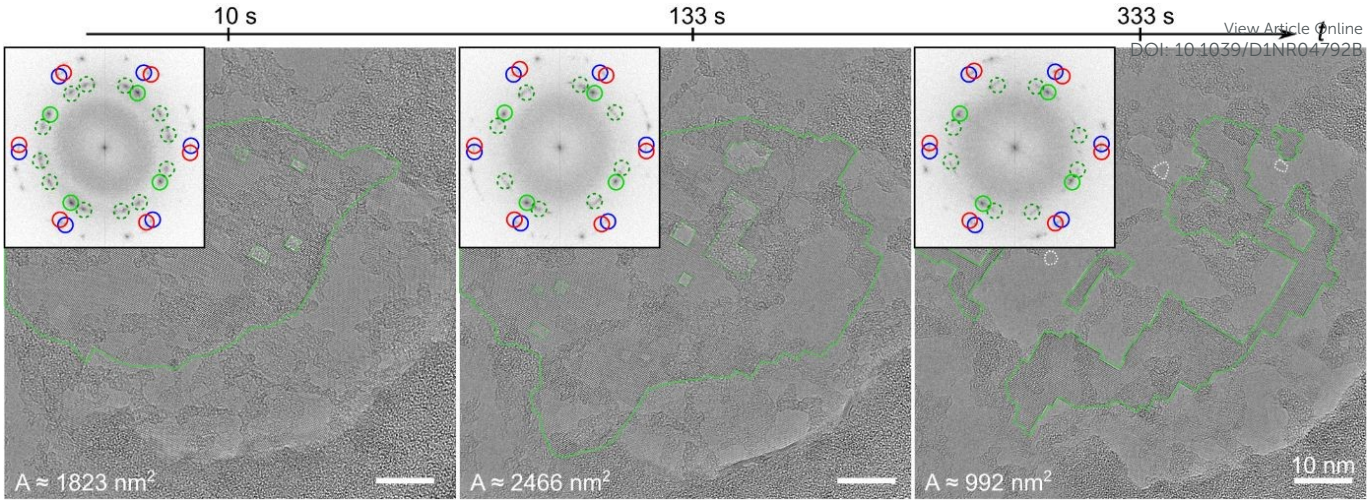

Figure 2: 80 kV Cs-corrected HRTEM image sequence of the 2500 nm²-sized NaCl crystal. Up to ~133 s, the crystal grows. Afterwards the crystal is decomposed. The dose rate was ~$2.5 \cdot 10^5$ e^-/nm^2s. In the inset, the FFTs are shown which indicate two layer of graphene (red, blue) and NaCl crystals where the dominant orientation is marked with solid green and other appearing orientations with dashed green circles. The dominant NaCl crystal is encircled green. Identified holes in graphene are marked white.

Further experiments on NaCl encapsulation were performed to make sure that the NaCl degradation is induced by appearance of defects in graphene (see Fig. S2 of the Supporting Information for additional examples). Another example of such a behaviour is presented in Fig. 2 for a larger crystal. First, the crystal grows up to a total accumulated dose of ~$5.8 \cdot 10^7$ e^-/nm^2 (see the first two panels of Fig. 2), which is then stable until a total dose of ~$7.1 \cdot 10^7$ e^-/nm^2 is reached and decomposes afterwards. The whole growth and degradation process is shown in the supplementary video, where the time evolution of the crystal is accelerated by a factor of ~15. For better visualization, the actual size of the NaCl crystal is marked with a green frame in Fig. 2 (b). The holes formed in graphene are encircled white. From this observation we can again conclude that the degradation is initiated by defect formation in graphene, similar to other encapsulated NaCl crystals. In the FFTs of the corresponding images, the graphene reflections are marked red and green. The main orientation of the NaCl reflections is marked green.

Further signals from other NaCl crystals appear in the FFT, see the additional NaCl reflections marked by green dashed circles. However, the additional reflections vanish, which could indicate a growth process of the framed NaCl due to a step-by-step reorientation of the smaller crystals to the bigger NaCl crystal as the reflections of other orientations in the FFTs disappear. Similar behaviour of crystals in liquid cells was also reported earlier.[35] When the NaCl crystal reached its maximum size, the growth does not necessarily stop, but the degradation rate is faster than the growth rate.

Again, in Figs. 1 and 2, the NaCl crystal degradation started in the areas where the graphene sheet was damaged (marked with white frames in Figs. 1 (b) and 2, respectively). Due to the high stability of graphene against ionization, radiolysis and knock-on damage up to electron-beam energies of about 85 keV, it is reasonable to assume that defects in graphene are produced by chemical etching.[27,28] It is likely that the etching process is also caused by the chlorine radicals as mentioned above, which are produced by the interaction of the electron beam with the NaCl crystal inside the graphene enclosure. When a first defect in the pristine graphene lattice is formed, the size of the defect can grow because the displacement threshold at the edge atoms is lowered and knock-on damage can take place.[37,39] Additionally, the etching process is also further enhanced on defects.[29,30] As soon as a first defect appears in graphene, the NaCl flake quickly decomposes.

In order to understand the mechanism of flake decomposition under the electron beam, we carried out DFT calculations aimed at assessing the displacement thresholds of Na as well as Cl atoms from the NaCl flake, as described at length below. Sputtering from the (100) basal plane and from the edges was considered. Following previous calculations,[7,40,41] initial kinetic energy was assigned to the recoil atom and the evolution of the system was modelled using molecular dynamics. The thinnest possible NaCl crystals consisting of two atomic planes were considered, which was metastable even as a free-standing system due to extremely low (about 10 meV/Å²) (100) surface energy of NaCl crystals, as also previously reported.[42] Although electronic excitations and charge accumulation may affect the behaviour of the material under electron beam,[43] these effects were not considered, as they must have been mitigated by conducting graphene sheets encapsulating the NaCl crystals.

However, the evaluation of the displacement threshold defined as the minimum kinetic energy the recoil atom should gain to be sputtered away from the crystal is more complicated for NaCl than for metallic or semiconducting systems with a smaller degree of ionicity. Indeed, contrary to, e.g., graphene, there is almost complete charge transfer from Na to Cl atoms in the crystal, so that the atoms are sputtered as ions, not neutral species, which in turn, gives rise to the long-ranged interaction between the atom and charged vacancy left in the crystal, and for the finite supercells, to spurious interaction of the sputtered atoms with the periodic images of the crystal.

Figure 1: 80 kV Cs-corrected HRTEM image series of the degradation process of a graphene- encapsulated NaCl crystal. (a) show the raw images over a total time t of 885 s. The dose rate was about ~$6.1 \cdot 10^5$ e^-/nm^2s. In the inset of the first panel, the FFT of the crystal and the corresponding reflections of the two encapsulating graphene layers (red and blue) and the NaCl (green) are marked. (b) shows the same image sequence as in (a) but with colour coding of the two encapsulating graphene layers and the NaCl crystal (we used the colours for the NaCl crystal and the graphene as marked in the FFT). The white frames show holes in graphene. They lead to immediate degradation of the close-by NaCl crystal (adapted from [46]).

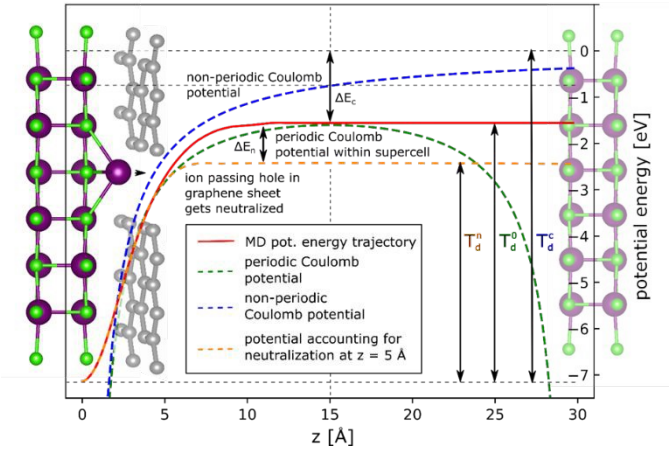

Figure 3: Schematic of the displacement threshold calculation for a charged recoil atom. Corrections due to the long ranged Coulombic interactions (blue dashed line) have to be considered. In the periodic supercell a periodic Coulomb potential (green dashed line) applies. Exemplarily the potential energy trajectory of an actual displacement of sodium atom is shown (red solid line). For a symmetrized supercell, the displacement is completed when the particle crosses the border to the next image cell, from the BO MD calculations the threshold T_d^0 can be obtained. The correction $T_d^c = T_d^0 + \Delta E_c$ to the non-periodic case can be found as the energy difference at the border $\Delta E_c = 2\left|V_{Coulomb}(q = q^*, z = L/2)\right|$, where q^* is the charge at the recoil (obtained by Bader analysis of the all-electron charge density) and L is the cell size in z-direction. The orange curve illustrates the situation when the recoil gets neutralized while passing through a hole in encapsulating graphene sheet, so that in this case the threshold energy is $T_d^n = T_d^0 - \Delta E_n$ with $\Delta E_n = \left|V_{Coulomb}(q = q^*, z = z_n) - V_{Coulomb}(q = q^*, z = L/2)\right|$.

In order to minimize the effects of the spurious long-range Coulomb interaction on the displacement threshold, the supercells, that is the vacuum area, must be infinitely large, which is in practice impossible due to computational limitations. In our DFT calculations, a supercell with a dimension of $L = 30$ Å in the transverse direction was chosen. Thus, a NaCl layer will interact with its image layer separated by 30 Å. This, in turn, should result in a change in the energy profile of the sputtered atom, that is the appearance of a maximum in the energy profile between the two layers at a distance $z = L/2$. Fig. 3 shows the emerging periodic Coulomb potential (green dashed line). The red solid line represents a resulting trajectory corresponding to the displacement threshold energy T_d^0, where the energy at a distance $z = L/2$ is sufficient to overcome the periodic Coulomb potential $\Delta E = V_{Coulomb}(q = q^*, z = L/2)$, where q^* is the charge at the recoil and L is the supercell size in z-direction. We found via Bader analysis that about 0.2 electrons remain on the sodium atom during the displacement process resulting in $Na^{0.8+}$ ($q^* = 0.8e$ with e as elementary charge) effectively. If a recoil atom (ion) passes the graphene sheet, it can pick up/lose some charge, as this process should be energetically favorable for both positively and negatively charge ions, since the empty or occupied electronic states in the ions should be lower/higher than the Fermi level in graphene, so that electron transfer process will be energetically favorable. The Coulomb interaction will be 'switched off', so that the displacement threshold energy becomes $T_d^n = T_d^0 - \Delta E_n$, the orange curve. Here $\Delta E_n = V_{Coulomb}(q = q^*, z = L/2) - V_{Coulomb}(q = q^*, z = z_n)$ denotes the energy gain caused by the neutralization at distance $z = z_n$, here z_n describe the distance at which the neutralization is completed, in our case for $z_n = 5$Å (distance between NaCl and graphene ~ 3.6 Å) we find $\Delta E_n = 1$eV. The correction of the displacement threshold energy T_d^c with a non-periodic Coulomb potential (blue dashed line) can be described as $T_d^c = T_d^0 + \Delta E_c$, with $\Delta E_c = 2\left|V_{Coulomb}(q = q^*, z = L/2)\right|$=1.2 eV.

Fig. 4 shows the displacement cross sections calculated using the McKinley-Feshbach formalism[44] for Na^+ (left panel) and Cl^- (right panel) with the displacement threshold energies evaluated under different assumptions (neutralization, no neutralization, sputtering from the basal plane or edges of NaCl crystals). Thermal vibrations are accounted for using the Debye model at a temperature of T= 300 K and a Debye temperature of T_{Debye} = 322 K.[45] The solid lines give the cross sections for the recoil atoms in the basal plane and the dashed lines for the edges. The results assuming neutralization of the recoil after passing the graphene are given in orange, with regard to a periodic Coulomb potential in green, and a non-periodic Coulomb potential in blue. Based on the determined displacement cross sections, it becomes evident that, with the used electron beam energy of 80 keV, knock-on damage on the NaCl crystal can appear in the basal plane but with a higher rate at the crystal edges, Fig. 4. Overall, the relatively high displacement rates indicate that free-standing NaCl crystals must quickly disintegrate under the 80 kV electron beam, emphasizing the importance of graphene sheets, which 'stop' the displaced atoms and make immediate

recombination of defects at the surface of the crystal possible. As can be seen from the HRTEM images in Fig. 1, crystal edges are also formed during the decomposition of NaCl as soon as a graphene hole appears. In this case, the edges are facing the formed hole in the graphene.

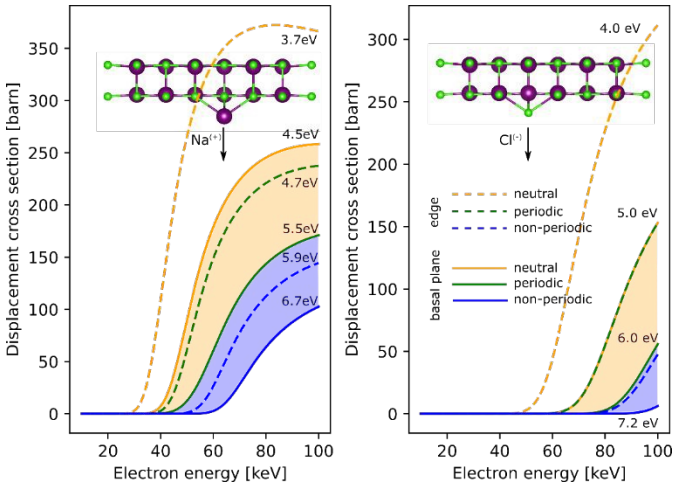

Figure 4: Displacement cross sections for sodium and chlorine atoms sputtered from bilayer NaCl under electron irradiation. The cross sections are calculated using the McKinley-Feshbach formula with account for thermal vibrations as described by the Debye model (T = 300 K, T_{Debye}=322 K). The cross sections from computed displacement thresholds are shown for the basal plane (solid) and edge (dashed) in green. The blue curves give a lower boundary for the displacement cross section, accounting for the increased threshold in the non-periodic situations. When accounting for the neutralization of the recoil by the passage of holes in graphene, the orange curves apply. Experiments are carried out for 80 keV, where displacement at the edges should be enhanced.

Furthermore, ionic crystals are susceptible to the electron beam via ionization and radiolysis[31]. However, as long as the displaced Na^+ and Cl^- ions are within the graphene enclosure, they can recombine again with the NaCl crystal either at their former position or fill other empty lattice spaces. This behaviour leads to the formation and movement of small rectangular defects within the NaCl structure, which can be observed in the supplementary video. This displacement and recombination do not contribute to the growth or degradation rate of the whole crystal but indicate a high mobility of the Na^+ and Cl^- ions within the graphene enclosure induced by ballistic energy transfer and radiolysis. When a hole in graphene appears, the migrating Na^+ and Cl^- ions can leave the encapsulation and will not necessarily recombine at other positions. Moreover, the Na^+ and Cl^- ions can cause further etching at the edges of the graphene defect and therefore lead to a defect growth as it can be deduced from Fig. 1 (b) based on the increasing hole size in graphene (white frames).

The projected NaCl crystal areas formed inside the GLCs were measured together with the total accumulated doses were measured until their disappearance for ten different NaCl crystals (see Fig. 5). For an easier comparison, the experimental datasets are normalized to the maximum projected area. Furthermore, each curve reflects a TEM image sequence of the full crystal lifetime where the projected area of the NaCl was measured in each image. It is striking that all the curves in Fig. 5 exhibit a sudden decay after a rather stable behaviour of the crystal. We notice further that some of the smaller crystals (85 nm², 90 nm², 105 nm²) have longer lifetime while the more extended crystals (1200 nm², 1215 nm², 2500 nm²) start to decompose very fast.

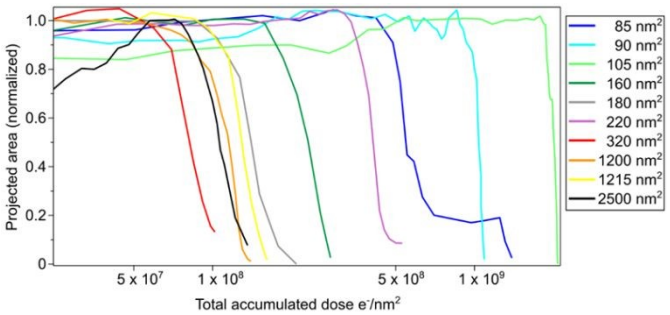

Figure 5: The projected area of NaCl crystals over the total accumulated dose. The crystals are normalized to their projected maximum size. Each crystal is stable up to a certain dose before it starts to decompose fast. All crystals show similar behaviour during the degradation process (adapted from [46]).

The 85 nm²-sized crystal shows the typical decay rate, but only until ~20% of the initial size is left. Then, it stabilizes at a total dose of ~$5 \cdot 10^8$ e^-/nm^2. It is very likely that this stabilization may occur due to graphene re-encapsulation so that the remaining NaCl crystal is again fully enclosed. After further electron beam irradiation, the remaining crystal, however, decomposes completely.

In general, all crystals show a similar decomposition behaviour, except for the most extended crystal (2500 nm²). In the beginning it grows as can be seen in the slope of the black curve before it shows the same decomposition behaviour like all the other crystals.

To quantify the degradation process of the crystals, a logistic decay function $f(x) = A/\left(1 + e^{k(\varphi - \varphi_{crit})}\right)$ is used. This function is determined by three parameters, the maximum value A, the slope k and the turning point at decay φ_{crit}, which is the critical dose where 50% of the initial crystal is decomposed. We normalized the data and A equals to 1. The parameter φ_{crit} reflects the stability of NaCl crystals. The larger φ_{crit} , the higher the total accumulated dose φ , which is taken before the degradation starts. By the slope k, the degradation rate per electron is determined. As an example, the data points (red) for the 220 nm² sized NaCl crystal with a corresponding fit of the logistic decay model (blue) are shown in the dashed framed inset of Fig. 6. The fit for the experimental data points works well up to a total dose of ~ $4.5 \cdot 10^8$ e^-/nm^2. After that a small deviation between fit and data points occurs, which can be explained by the remained NaCl crystal at the edges of the graphene encapsulation.

The green curve in Fig. 6 depicts the derivative of the fit. At the turning point φ_{crit} of the derivative, approximately 50% of the initial NaCl crystal is destroyed. Based on the turning point of the derivative, the critical dose is also determined. The turning point of the derivative represents also the highest rate of degradation, which is crystal size dependent (see discussion in the SI). All determined

values for the crystals are given in table S1 of the Supporting Information. For the crystal with size 320 nm² the highest rate of degradation was measured. This crystal started to decompose at two positions simultaneously, which could indicate that the protecting graphene was damaged at different positions. With the exception of the 320 nm² crystal, we could not identify any further significant dependence between the number of defects/holes in the graphene and the induced degradation rates of the other NaCl crystals.

For better visualization, the different crystals are given in Fig. 6 with their sizes and the corresponding critical doses φ_{crit} (red dots). It is striking that the three largest crystals (1200 nm², 1215nm², 2500nm²) survive only a very short exposure with the electron beam compared to other crystals with typical sizes $\leq$ 220 nm². We explain this behaviour with a probability per area for the appearance of a first defect in graphene, which initiate the decomposition of the whole NaCl crystal resulting in a shorter lifetime of larger graphene-encapsulated NaCl crystals.

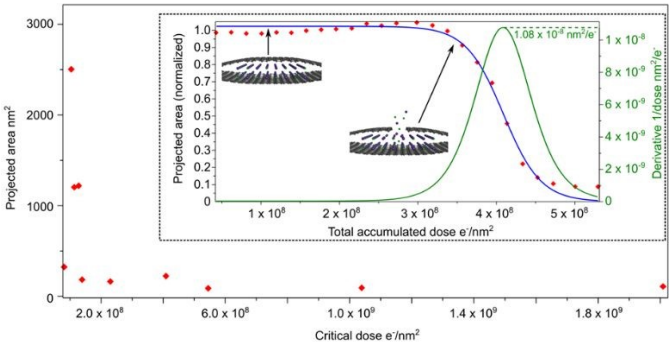

Figure 6: Projected crystal size versus critical dose, which is determined to be the dose where approximately 50% of the crystal is decomposed. The dashed framed inset shows a data point fit of the 220 nm² sized NaCl crystal. The experimental points were fitted with a logistic decay model (blue). As long as the blue curve remains constant the graphene encapsulation is intact. But the NaCl crystal gets immediately decomposed when a hole in the encapsulating graphene appears. The negative derivative is shown (green) which was used to get the slope of the highest degradation during the whole process as well as the turning point, which corresponds to the critical dose.

C Experimental

Sample preparation

Chemical vapor deposited (CVD) graphene on copper was used for the preparation of the liquid cells.[47] Two TEM gold grids (Quantifoil R1.2/1.3) were placed, together with a drop of isopropyl alcohol (C_3H_8O), on the surface of the graphene covered copper. Due to the evaporation of the isopropyl alcohol, the TEM grids adhere to the surface of the graphene on the copper substrate. Afterwards, the copper was etched away with a 0.25 M ammonium peroxidisulphate (APS) solution. Thus, the grids with the graphene remained on the APS solution. In the next step the grids with the graphene were lifted out with a sieve and cleaned with pure water. For the NaCl encapsulation, an approach similar to the preparation of a graphene liquid cell was used. A drop (~1 µl) of the 0.01 M – 0.05 M NaCl solution is put between two TEM grids with transferred CVD graphene facing to each other. During the evaporation of the water, the grids are coming into contact and encapsulate remaining NaCl solution as well as the investigated NaCl crystals, which are formed due to supersaturation. Thus, vertical heterostructures consisting of graphene and NaCl are formed.

Imaging conditions

For the imaging experiments in the high-resolution TEM mode, a third order spherical aberration (Cs) – corrected FEI Titan 80-300 was used. The acceleration voltage was 80 kV and the experiments were performed with dark atom contrast. Moreover, the value for the spherical aberration was set to *Cs* ≈ 20 µm and the extraction voltage of the gun was 2000 V. The images were acquired with dose rates in the order of 10^6 e/(nm²s) and a vacuum level of 10^{-5} Pa. Furthermore, it is assumed that the specimen and the sample holder are at near-ambient temperature. The recorded images were post-processed with the "Orientation Mapping" plugin for ImageJ to include a color-coding for visualization of the different crystals.[48]

Computational Methods

The displacement thresholds were calculated using DFT Born-Oppenheimer molecular dynamics simulations as implemented in the VASP code.[49] An atom in the simulations was considered to be displaced when it moved across the boundary of the supercell in z-direction (perpendicular to the bilayer NaCl). The displacement threshold T_d^0 obtained in the periodic setup was then corrected for the Coulombic interaction between images in the supercell approach. The time step in the MD simulation run was set to 0.2 fs for 1000 steps, afterwards the time step was increased to 1.0 fs due to the low velocity of the recoil when approaching the top of the potential barrier. The simulations were carried out using the PBE-GGA functional, 5x5x1 k points sampling and a plane wave cut-off of 300 eV in a 6x6 supercell (corresponding to 36 Na and 36 Cl atoms).

Conclusions

To summarize, we investigated the stability of thin NaCl crystals encapsulated between graphene under electron beam irradiation during TEM imaging and showed that NaCl, which, is strongly electron-radiation-sensitive when unprotected, is stable between graphene as long as the graphene sheets are not damaged. This behaviour was confirmed by DFT calculations. We found that the formed NaCl crystals decompose immediately when the first defect in graphene appears. Regarding the dose-dependent lifetime, we found that large crystals ($\geq$ 1200 nm²) decompose earlier and faster than smaller ones ($\leq$ 220 nm²). We explained this behaviour with the probability of defect formation per graphene area under the electron beam: The larger the encapsulating graphene area, the higher the probability that a point defect is produced, which then causes immediate decomposition of the encapsulated NaCl crystal. Our results provide quantitative data on the stability of encapsulated quasi 2D NaCl crystals and indicate that only high-quality graphene is suitable for protecting ionic crystals from beam damage in electron

microscopy studies. We expect that these new insights on the stability of the materials between graphene sheets will not only contribute to the better protection of quasi-2D inorganic solids, but also be relevant to the protection of liquids and organic molecules, and thus make future in-situ electron microscopy experiments possible on these systems.

Conflicts of interest

There are no conflicts to declare.

Acknowledgements

We acknowledge funding from the German Research Foundation (DFG) in the frame of the project 345789964 as well as project KR 48661/1, and through the collaborative research centre "Chemistry of Synthetic 2D Materials" SFB-1415-417590517. We further thank the Gauss Centre for Supercomputing e.V. (www.gauss-centre.eu) for providing computing time on the GCS Supercomputer HAWK at Höchstleistungsrechenzentrum Stuttgart (www.hlrs.de) and also TU Dresden (Taurus cluster) for generous grants of CPU time.

Notes and references

(1) Lee, C.; Wei, X.; Kysar, J. W.; Hone, J. Measurement of the Elastic Properties and Intrinsic Strength of Monolayer Graphene. *Science (80-.).* **2008**, *321* (5887), 385–388.

(2) Ghosh, dS; Calizo, I.; Teweldebrhan, D.; Pokatilov, E. P.; Nika, D. L.; Balandin, A. A.; Bao, W.; Miao, F.; Lau, C. N. Extremely High Thermal Conductivity of Graphene: Prospects for Thermal Management Applications in Nanoelectronic Circuits. *Appl. Phys. Lett.* **2008**, *92* (15), 151911.

(3) Neto, A. H. C.; Guinea, F.; Peres, N. M. R.; Novoselov, K. S.; Geim, A. K. The Electronic Properties of Graphene. *Rev. Mod. Phys.* **2009**, *81* (1), 109.

(4) Balandin, A. A.; Ghosh, S.; Bao, W.; Calizo, I.; Teweldebrhan, D.; Miao, F.; Lau, C. N. Superior Thermal Conductivity of Single-Layer Graphene. *Nano Lett.* **2008**, *8* (3), 902–907.

(5) Zhang, Y. I.; Zhang, L.; Zhou, C. Review of Chemical Vapor Deposition of Graphene and Related Applications. *Acc. Chem. Res.* **2013**, *46* (10), 2329–2339.

(6) Park, S.; Ruoff, R. S. Chemical Methods for the Production of Graphenes. *Nat. Nanotechnol.* **2009**, *4* (4), 217.

(7) Meyer, J. C.; Eder, F.; Kurasch, S.; Skakalova, V.; Kotakoski, J.; Park, H. J.; Roth, S.; Chuvilin, A.; Eyhusen, S.; Benner, G.; et al. Accurate Measurement of Electron Beam Induced Displacement Cross Sections for Single-Layer Graphene. *Phys. Rev. Lett.* **2012**, *108* (19), 196102.

(8) Yuk, J. M.; Park, J.; Ercius, P.; Kim, K.; Hellebusch, D. J.; Crommie, M. F.; Lee, J. Y.; Zettl, A.; Alivisatos, A. P. High-Resolution EM of Colloidal Nanocrystal Growth Using Graphene Liquid Cells. *Science (80-.).* **2012**, *336* (6077), 61–64.

(9) De Clercq, A.; Dachraoui, W.; Margeat, O.; Pelzer, K.; Henry, C. R.; Giorgio, S. Growth of Pt--Pd Nanoparticles Studied in Situ by HRTEM in a Liquid Cell. *J. Phys. Chem. Lett.* **2014**, *5* (12), 2126–2130.

(10) Nguyen, L.; Komsa, H.-P.; Khestanova, E.; Kashtiban, R. J.; Peters, J. J. P.; Lawlor, S.; Sanchez, A. M.; Sloan, J.; Gorbachev, R. V; Grigorieva, I. V; et al. Atomic Defects and Doping of Monolayer NbSe2. *ACS Nano* **2017**, *11* (3), 2894–2904.

(11) Cao, Y.; Mishchenko, A.; Yu, G. L.; Khestanova, E.; Rooney, A. P.; Prestat, E.; Kretinin, A. V; Blake, P.; Shalom, M. Ben; Woods, C.; et al. Quality Heterostructures from Two-Dimensional Crystals Unstable in Air by Their Assembly in Inert Atmosphere. *Nano Lett.* **2015**, *15* (8), 4914–4921.

(12) Chen, Q.; Smith, J. M.; Park, J.; Kim, K.; Ho, D.; Rasool, H. I.; Zettl, A.; Alivisatos, A. P. 3D Motion of DNA-Au Nanoconjugates in Graphene Liquid Cell Electron Microscopy. *Nano Lett.* **2013**, *13* (9), 4556–4561.

(13) Algara-Siller, G.; Lehtinen, O.; Wang, F. C.; Nair, R. R.; Kaiser, U.; Wu, H. A.; Geim, A. K.; Grigorieva, I. V. Square Ice in Graphene Nanocapillaries. *Nature* **2015**, *519* (7544), 443.

(14) Elibol, K.; Susi, T.; Argentero, G.; Reza Ahmadpour Monazam, M.; Pennycook, T. J.; Meyer, J. C.; Kotakoski, J. Atomic Structure of Intrinsic and Electron-Irradiation-Induced Defects in MoTe2. *Chem. Mater.* **2018**, *30* (4), 1230–1238.

(15) Zan, R.; Ramasse, Q. M.; Jalil, R.; Georgiou, T.; Bangert, U.; Novoselov, K. S. Control of Radiation Damage in MoS by Graphene Encapsulation. *ACS Nano* **2013**, No. 11, 1–17. https://doi.org/10.1021/nn4044035.

(16) Lehnert, T.; Lehtinen, O.; Algara--Siller, G.; Kaiser, U. Electron Radiation Damage Mechanisms in 2D MoSe2. *Appl. Phys. Lett.* **2017**, *110* (3), 33106.

(17) Algara-Siller, G.; Kurasch, S.; Sedighi, M.; Lehtinen, O.; Kaiser, U. The Pristine Atomic Structure of MoS$_2$ Monolayer Protected from Electron Radiation Damage by Graphene. *Appl. Phys. Lett.* **2013**, *103* (20). https://doi.org/http://dx.doi.org/10.1063/1.4830036.

(18) Textor, M.; de Jonge, N. Strategies for Preparing Graphene Liquid Cells for Transmission Electron Microscopy. *Nano Lett.* **2018**, *18* (6), 3313–3321.

(19) Chamberlain, T. W.; Biskupek, J.; Skowron, S. T.; Markevich, A. V; Kurasch, S.; Reimer, O.; Walker, K. E.; Rance, G. A.; Feng, X.; Müllen, K.; et al. Stop-Frame Filming and Discovery of Reactions at the Single-Molecule Level by Transmission Electron Microscopy. *ACS Nano* **2017**, *11* (3), 2509–2520.

(20) Shin, D.; Park, J. B.; Kim, Y.-J.; Kim, S. J.; Kang, J. H.; Lee, B.; Cho, S.-P.; Hong, B. H.; Novoselov, K. S. Growth Dynamics and Gas Transport Mechanism of Nanobubbles in Graphene Liquid Cells. *Nat. Commun.* **2015**, *6* (1), 1–6.

(21) Egerton, R. F.; Li, P.; Malac, M. Radiation Damage in the TEM and SEM. *Micron* **2004**, *35* (6), 399–409. https://doi.org/10.1016/j.micron.2004.02.003.

(22) Zobelli, A.; Gloter, A.; Ewels, C. P.; Seifert, G.; Colliex, C. Electron Knock-on Cross Section of Carbon and Boron Nitride Nanotubes. *Phys. Rev. B* **2007**, *75* (24), 245402.

(23) Banhart, F. Irradiation Effects in Carbon Nanostructures. *Reports Prog. Phys.* **1999**, *62* (8), 1181.

(24) Reimer, L. *Transmission Electron Microscopy: Physics of Image Formation and Microanalysis*; Springer, 2013; Vol. 36.

(25) Talmon, Y. Electron Beam Radiation Damage to Organic and Biological Cryospecimens. In *Cryotechniques in*

Biological Electron Microscopy; Springer, 1987; pp 64–84.

(26) Cho, H.; Jones, M. R.; Nguyen, S. C.; Hauwiller, M. R.; Zettl, A.; Alivisatos, A. P. The Use of Graphene and Its Derivatives for Liquid-Phase Transmission Electron Microscopy of Radiation-Sensitive Specimens. *Nano Lett.* **2017**, *17* (1), 414–420.

(27) Thiele, C.; Felten, A.; Echtermeyer, T. J.; Ferrari, A. C.; Casiraghi, C.; Löhneysen, H. v; Krupke, R. Electron-Beam-Induced Direct Etching of Graphene. *Carbon N. Y.* **2013**, *64*, 84–91.

(28) Mølhave, K.; Gudnason, S. B.; Pedersen, A. T.; Clausen, C. H.; Horsewell, A.; Bøggild, P. Electron Irradiation-Induced Destruction of Carbon Nanotubes in Electron Microscopes. *Ultramicroscopy* **2007**, *108* (1), 52–57.

(29) Ramasse, Q. M.; Zan, R.; Bangert, U.; Boukhvalov, D. W.; Son, Y.-W.; Novoselov, K. S. Direct Experimental Evidence of Metal-Mediated Etching of Suspended Graphene. *ACS Nano* **2012**, *6* (5), 4063–4071.

(30) Leuthner, G. T.; Hummel, S.; Mangler, C.; Pennycook, T. J.; Susi, T.; Meyer, J. C.; Kotakoski, J. Scanning Transmission Electron Microscopy under Controlled Low-Pressure Atmospheres. *Ultramicroscopy* **2019**.

(31) Hobbs, L. W. Radiation Effects in Analysis of Inorganic Specimens by TEM. In *Introduction to Analytical Electron Microscopy*; Springer, 1979; pp 437–480.

(32) Egerton, R. Radiation Damage and Nanofabrication in TEM and STEM. *Micros. Today* **2021**, *29* (3), 56–59.

(33) Ye, X.; Jones, M. R.; Frechette, L. B.; Chen, Q.; Powers, A. S.; Ercius, P.; Dunn, G.; Rotskoff, G. M.; Nguyen, S. C.; Adiga, V. P.; et al. Single-Particle Mapping of Nonequilibrium Nanocrystal Transformations. *Science (80-.).* **2016**, *354* (6314), 874–877.

(34) Vasu, K. S.; Prestat, E.; Abraham, J.; Dix, J.; Kashtiban, R. J.; Beheshtian, J.; Sloan, J.; Carbone, P.; Neek-Amal, M.; Haigh, S. J.; et al. Van Der Waals Pressure and Its Effect on Trapped Interlayer Molecules. *Nat. Commun.* **2016**, *7*, 12168.

(35) Lehnert, T.; Kinyanjui, M. K.; Ladenburger, A.; Rommel, D.; Wörle, K.; Börrnert, F.; Leopold, K.; Kaiser, U. In Situ Crystallization of the Insoluble Anhydrite AII Phase in Graphene Pockets. *ACS Nano* **2017**, *11* (8), 7967–7973.

(36) Zhou, W.; Yin, K.; Wang, C.; Zhang, Y.; Xu, T.; Borisevich, A.; Sun, L.; Idrobo, J. C.; Chisholm, M. F.; Pantelides, S. T.; et al. The Observation of Square Ice in Graphene Questioned. *Nature* **2015**, *528* (7583), E1.

(37) Girit, Ç. Ö.; Meyer, J. C.; Erni, R.; Rossell, M. D.; Kisielowski, C.; Yang, L.; Park, C.-H.; Crommie, M. F.; Cohen, M. L.; Louie, S. G.; et al. Graphene at the Edge: Stability and Dynamics. *Science (80-.).* **2009**, *323* (5922), 1705–1708.

(38) Crespi, V. H.; Chopra, N. G.; Cohen, M. L.; Zettl, A.; Louie, S. G. Anisotropic Electron-Beam Damage and the Collapse of Carbon Nanotubes. *Phys. Rev. B* **1996**, *54* (8), 5927.

(39) Susi, T.; Kotakoski, J.; Arenal, R.; Kurasch, S.; Jiang, H.; Skakalova, V.; Stephan, O.; Krasheninnikov, A. V; Kauppinen, E. I.; Kaiser, U.; et al. Atomistic Description of Electron Beam Damage in Nitrogen-Doped Graphene and Single-Walled Carbon Nanotubes. *ACS Nano* **2012**, *6* (10), 8837–8846.

(40) Komsa, H.-P.; Kotakoski, J.; Kurasch, S.; Lehtinen, O.; Kaiser, U.; Krasheninnikov, A. V. Two-Dimensional Transition Metal Dichalcogenides under Electron Irradiation: Defect Production and Doping. *Phys. Rev. Lett.* **2012**, *109* (3), 35503.

(41) Pizzochero, M.; Yazyev, O. V. Single-Layer 1T MoS2 under Electron Irradiation from Ab Initio Molecular Dynamics. *2D Mater.* **2018**, *5* (2), 25022.

(42) Kvashnin, A. G.; Kvashnin, D. G.; Oganov, A. R. Novel Unexpected Reconstructions of (100) and (111) Surfaces of NaCl: Theoretical Prediction. *Sci. Rep.* **2019**, *9* (1), 1–9.

(43) Kretschmer, S.; Lehnert, T.; Kaiser, U.; Krasheninnikov, A. V. Formation of Defects in Two-Dimensional MoS2 in the Transmission Electron Microscope at Electron Energies below the Knock-on Threshold: The Role of Electronic Excitations. *Nano Lett.* **2020**.

(44) McKinley, W. A.; Feshbach, H. The Coulomb Scattering of Relativistic Electrons by Nuclei. *Phys. Rev.* **1948**, *74* (12), 1759–1763. https://doi.org/10.1103/PhysRev.74.1759.

(45) Raunio, G.; Rolandson, S. Lattice Dynamics of Nacl, Kcl, Rbcl, and Rbf. *Phys. Rev. B* **1970**, *2* (6), 2098.

(46) Lehnert, T. Electron-Beam-Induced Modifications in Two-Dimensional Materials, Universität Ulm, 2020.

(47) Cho, Y.; Yang, J.-M.; Lee, S.-M.; Kim, J.-H.; Han, K.-Y.; Chang, J.; others. Transmission Electron Microscopy Specimen Preparation for Layer-Area Graphene by a Direct Transfer Method. *Appl. Microsc.* **2014**, *44* (4), 133–137.

(48) Lehtinen, O.; Komsa, H.-P.; Pulkin, A.; Whitwick, M. B.; Chen, M.-W.; Lehnert, T.; Mohn, M. J.; Yazyev, O. V.; Kis, A.; Kaiser, U.; et al. Atomic Scale Microstructure and Properties of Se-Deficient Two-Dimensional MoSe $_2$. *ACS Nano* **2015**, *9* (3), 3274–3283. https://doi.org/10.1021/acsnano.5b00410.

(49) Kresse, G.; Furthmüller, J. Efficient Iterative Schemes for Ab Initio Total-Energy Calculations Using a Plane-Wave Basis Set. *Phys. Rev. B* **1996**, *54* (16), 11169.